Ocean Dynamics (2016) 66:1715–1732
DOI 10.1007/s10236-016-1002-7

Tide-surge and wave interaction in the Gulf of Maine during an extratropical storm

Qingping Zou[1] · **Dongmei Xie**[1]

Received: 16 March 2016 / Accepted: 20 September 2016 / Published online: 13 October 2016

Abstract The fully coupled spectral wave and circulation model SWAN + ADCIRC was applied to investigate tide-surge and wave interaction in the Gulf of Maine during the extratropical storm on Patriot's Day of 2007. Significant tide-surge and wave interaction was found over Georges Bank and in the coastal areas. Over Georges Bank, the wave-induced current reached 0.2 m/s at the storm peak, accounting for 17 % of the total depth-averaged current. In Saco Bay, the current was dominated by wave-induced current with a magnitude up to 1.0 m/s during the storm. Two clockwise circulation gyres were found to form and sustain over a period of 26 hours during the storm in the bay. They were driven by spatial variations of wave height, direction and the resulting wave radiation stress gradient. Wave setup reached 0.2 m at the storm peak along the coast of Saco Bay. In Saco Bay, wave energy dissipation was reduced and wave height increased due to the increased water depth at high tide and surge. Therefore, wave height was modulated by tide and surge accordingly along the coast. As a result, wave setup and wave-induced current in the bay were also modulated by tide and surge. During the tidal cycle at the storm peak, wave setup increased with tidal level and the maximum wave setup coincided with high tide.

This article is part of the Topical Collection on *the 14th International Workshop on Wave Hindcasting and Forecasting in Key West, Florida, USA, November 8–13, 2015*

Responsible Editor: Kevin Horsburgh

✉ Qingping Zou
qingping.zou@maine.edu

[1] Department of Civil and Environmental Engineering, University of Maine, Orono, ME 04469-5711, USA

Keywords SWAN · ADCIRC · The Gulf of Maine · Tide-surge · Waves · Georges Bank · Saco Bay · Wave induced current

1 Introduction

The interaction among tide, surge, and waves during storm events can be significant in shallow waters where it is enhanced by the complicated bathymetric features and geometric configurations (e.g., Wolf 2009; Nicolle et al. 2009). Accurate prediction of water level and waves in coastal areas, especially low-lying areas prone to flooding requires better understanding of these processes (Zou et al. 2013). Tide-surge and wave interaction was also found to have significant impact on sediment transport in the littoal zone (e.g., Warner et al. 2008, 2010).

Tide-surge and waves interact with each other through their influences on the mean water depth/water level and currents. Wave and current in turn are coupled through wave radiation stress (e.g., Longuet-Higgins and Stewart 1962, 1964; Zou et al. 2006; Ardhuin et al. 2008; Mellor 2005, 2008), bottom stress (e.g., Grant and Madsen 1979; Zou 2004), and surface stress in the presence of waves (e.g., Johnson et al. 1998; Taylor and Yelland 2001; Moon et al. 2004a, b; Haus 2007). The mechanisms of tide-surge and wave interaction were summarized in several papers (e.g., Ozer et al. 2000; Wolf 2009).

In addition, it is well-known that waves give rise to near-surface drift currents known as the Stokes drift. Wind-generated surface currents are modified by wind-wave and wave-current momentum transfer (e.g., Jenkins 1986, 1987a, b, 1989). The total surface current is the sum of the wave modified current, the Stokes drift and the tidal current (e.g., Perrie et al. 2003; Tang et al. 2007). While 3D wave radiation stress has been derived (e.g., Mellor 2005, 2008; Ardhuin et al. 2008), the 2D wave radiation stress by Longuet-Higgins and

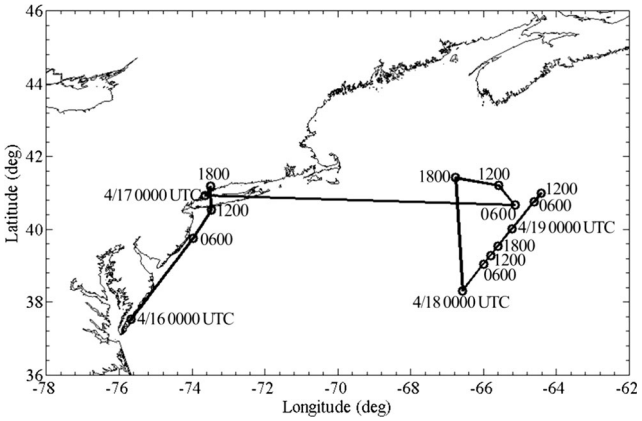

Fig. 1 Storm track of the 2007 Patriot's Day storm created by NCEP North American Regional Reanalysis meteorological data. The *circles* are the locations of the storm center at every 6-hourly time interval from 0000UTC 4/16/2007 to 1200 UTC 4/19/2007

Stewart (1962, 1964) is still widely used (e.g., Dietrich et al. 2012; Bolaños et al. 2014). In shallow water, wave propagation and transformation is strongly dependent on water depth and therefore on tide and surge level. Currents also cause a Doppler shift of wave frequency and refraction due to horizontal current and current gradients (Komen et al. 1996).

In the coastal area, waves contribute to water level through wave setup and drive longshore and cross-shore current due to the excess momentum flux induced by waves, which is parameterized as wave radiation stress (Longuet-Higgins and Stewart 1961, 1962, 1964; Xia et al. 2004; Zou et al. 2006; Mellor, 2005, 2008; Ardhuin et al. 2008; Bennis et al. 2011; Sheng and Liu 2011). Waves affect surge generation through wave-induced surface roughness and stress (e.g., Janssen 1989, 1991; Craig and Banner 1994; Brown and Wolf 2009). In shallow water, waves enhance the bottom friction experienced by currents (e.g., Grant and Madsen 1979; Christoffersen and Jonsson 1985; Xie et al. 2001; Zou 2004). Many other studies of wave-current interaction have been carried out previously, e.g., Perrie et al. (2003), Tang et al. (2007) and Uchiyama et al. (2009, 2010).

In this paper, we mainly focus on addressing tide-surge and wave interaction in shallow water areas in the Gulf of Maine, where the impact of currents, waves, and surges is closely linked. Since wave radiation stress is only significant where wave height changes drastically due to wave energy dissipation by wave breaking and bottom friction, its impact on mean current in the deep ocean is negligible.

The Gulf of Maine is an area frequently attacked by nor'easters, the intense, extratropical storms with a prolonged northeast fetch off the Atlantic which generate large waves and elevated water level and cause coastal flooding. The Patriot's Day storm in April 2007 is a notable example of nor'easters. The lowest central barometric pressure recorded was 968 hPa, with its intensity similar to a moderate category II hurricane. The storm took a dangerous path towards the coastline (Fig. 1) and swept through the northeastern USA during April 15–18, 2007. It became quasi-stationary near New York City in the morning of April 16, generating persisting strong southeast wind in the Gulf of Maine, with its peak wind gust above 70 m/s (Marrone 2008). The storm quickly weakened and moved to the east on April 17. It intensified again on April 18

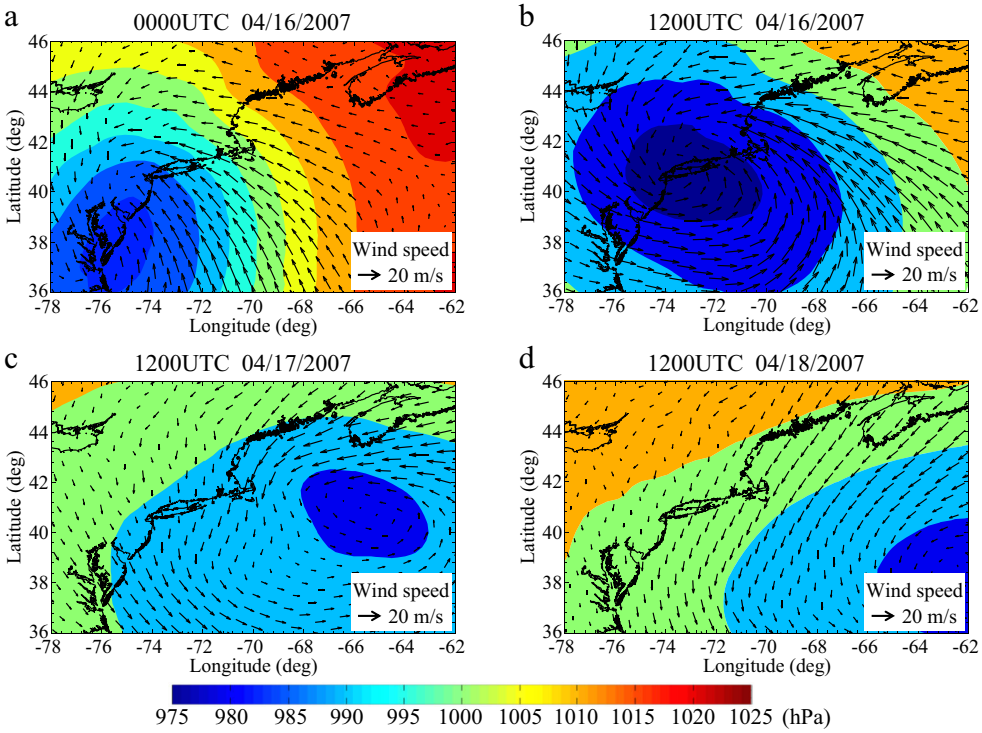

Fig. 2 Time evolution of pressure and wind fields during the Patriot's Day storm by NCEP North American Regional Reanalysis meteorological data from April 16 to April 18, 2007. The color maps illustrate atmospheric pressure at the sea surface. The vectors represent the wind field at 10 m above the sea surface

and produced strong northeast wind in the Gulf of Maine (Fig. 1 and Fig. 2).

The storm generated a pronounced storm surge and large waves along the western periphery of the Gulf of Maine. The combination of high astronomical tides, storm surge, and large battering waves resulted in significant coastal flooding and severe erosion along the vulnerable sandy coastline from southern Maine through Cape Cod, Massachusetts. The storm tide near Portland exceeded that of the 1991 "Perfect Storm." The widespread and severe coastal flooding caused an estimated $22 million in damage to public coastal infrastructure (Marrone 2008).

The reliable prediction of storm surge and waves in the Gulf of Maine remains a major challenging issue due to the complex bathymetry and topography and large tidal range in this region. The accuracy of the wave and surge forecasts is largely dependent on the quality of ocean bathymetry and meteorological forcing that drives the model. Maine has an extremely complex coastline and rapidly changing bathymetry on all scales, so both wind and wave fields are subject to drastic changes along the coast. Wave propagation, growth, and dissipation will be heavily influenced by the local wind, bathymetry, and surrounding islands (Panchang et al. 2008).

In the past, the numerical studies of tide-surge and waves in the Gulf of Maine have been carried out separately and mainly on nested structured grids. For example, Panchang et al. (2008) conducted numerical simulation on waves and analyzed wave climate in the Gulf of Maine. In this study, they coupled NOAA's open ocean wave predictions to two coastal, high-resolution, regional, and local domain structured grids. Bernier and Thompson (2007) used a modified version of the Princeton Ocean Model to investigated tide-surge interaction in the Gulf of Maine. Only recently, a fully coupled circulation and wave model, FVCOM/SWAVE on unstructured grids (Sun et al. 2013; Beardsley et al. 2013; Chen et al. 2013) was applied to study waves and circulation in the Gulf of Maine. Sun et al. (2013) investigated the effect of wave-current interaction on storm surge prediction. Chen et al. (2013) evaluated the performance of three fully coupled current-wave ocean models (ADCIRC/SWAN, FVCOM/SWAVE, SELFE/WWM) in predicting the coastal inundation at Scituate harbor, Massachusetts, during two nor'easters including the 2007 Patriot's Day storm.

Panchang et al. (2008) pointed out that due to the large tidal range in Maine, the tidal currents are likely to have significant impact on wave propagation. Up to now, however, there is little knowledge of the tide and current effects on waves in the Gulf of Maine. Only very recently, Sun et al. (2013) investigated the wave-current interaction during Hurricane Bob using FVCOM/SWAVE model. But for this particular storm, they found little tidal effect on surface waves. Xie et al. (2016) applied ADCIRC and SWAN to study tide-surge and waves, respectively, without considering wave-current interaction at the coast of Gulf of Maine. In this paper, we will examine the tide-surge effect on waves at the coastal areas of Maine during the Patriot's Day storm.

The tide-surge model ADCIRC coupled with the nearshore spectral wave model SWAN on the same shared unstructured mesh will be used in this study. ADCIRC's finite element method-based approach enables a large number of discrete points to be placed in a highly flexible and unstructured fashion with high resolution in coastal regions and low resolution in deep ocean. The complex bathymetry and topography of the coast of Maine including the nearby mainland, islands, jetty, and other structures is best captured in this way. Numerous studies have shown this model to be accurate for computing the variations in water level during extreme events throughout the Western North Atlantic and Gulf of Mexico region (Luettich et al. 1994; Mukai et al. 2001; Westerink et al. 2008). Zijlema (2010) developed and tested an updated version of SWAN on unstructured grids.

Currently, there is a lack of comprehensive study of tide-surge and wave interaction throughout the Gulf of Maine. The objective of this paper is to better understand the coupling between tide-surge and waves during an extratropical storm such as the 2007 Patriot's Day storm in the Gulf of Maine, with special attention to Georges Bank and Saco Bay. The former is one of the most productive shelf ecosystems in the world (Fry 1988) and the latter has suffered from severe erosion in the past decades (Hill et al. 2004).

The paper is organized as follows. A brief description of the fully coupled tide-surge-wave model SWAN + ADCIRC and model setup are given in Section 2. In Section 3, the model prediction is validated against the measurements. The tide-surge and wave interaction in the Gulf of Maine is evaluated based on model results and discussed in Section 4. Finally, conclusions and discussions are presented in Section 5.

2 eSWAN + ADCIRC model

2.1 Model description

The ADvanced CIRCulation (ADCIRC) model was used to simulate the response of water level and currents in the Gulf of Maine during the 2007 Patriot's Day storm. The model was originally developed by Luettich et al. (1992) and Westerink et al. (1994). The 2-D depth-integrated version, often referred to as ADCIRC-2DDI, was used in this work. This model solves generalized wave continuity equations on an unstructured finite element mesh with a continuous Galerkin finite-element formation. By using an unstructured triangular mesh, the model provides considerable flexibility in resolving complex geometry and bathymetry. The ADCIRC-2DDI is particularly suitable for predicting storm surge and coastal inundation with high computing efficiency (Luettich et al. 1992; Westerink et al. 1994; Dietrich et al. 2012). It has been implemented to model coastal circulation by Chen et al. (2008) and Dietrich et al. (2010). In this paper, we mainly focus on wave-current interaction in relatively shallow water areas, i.e., Georges Bank and Saco Bay, where the 2-D model is appropriate.

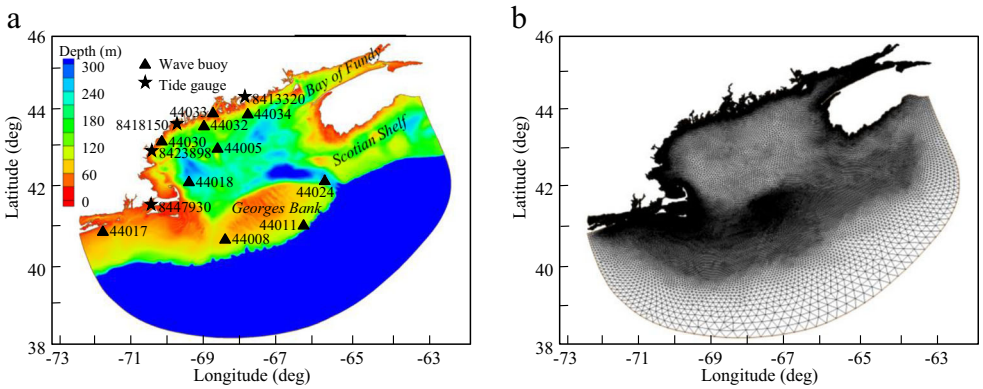

Fig. 3 Model domain covering the Gulf of Maine. **a** Bathymetry, wave buoys (*black triangle*) and tide gauges (*black star*). **b** Finite element mesh

The third-generation spectrum wave model Simulating WAves Nearshore (SWAN) model is a third-generation phase averaged wave model that computes random, short-crested wind-generated waves in coastal regions and inland water based on wind, bottom topography, currents, and tides (Booij et al. 1999; Ris et al. 1999).The SWAN model accounts for wave triad and quartet interactions, depth-induced wave breaking, bottom friction, and whitecapping dissipation. It solves the wave action balance equation and obtains wave parameters by integrating the two-dimensional wave energy spectrum in the frequency and direction domain. Zijlema (2010) developed a new unstructured grid procedure for the spectral wind-wave model SWAN. The unstructured grid version of SWAN uses a vertex-based, fully implicit, finite difference method which can accommodate unstructured meshes with a high variability in geographic resolution. Although the unstructured version of SWAN is numerically stable in time integration which adopts the first order implicit Euler scheme, the model results may also be improved by reducing the time step based on our sensitivity tests and previous study by Zijlema (2010).

ADCIRC and SWAN share the same unstructured finite element mesh when they are coupled. ADCIRC interpolates the input wind spatially and temporally onto the computational vertices to calculate water level and currents. The wind field, water level, and currents are then passed to the SWAN model. SWAN is run on the same interval, using the average of the ADCIRC variables from the interval in its computations to predict directional wave spectra by solving the wave action density balance equation. After its time step, SWAN computes the radiation stress gradients and passes them to ADCIRC, which then begins the process anew on the next interval (Dietrich et al. 2011). The radiation stress (Longuet-Higgins and Stewart 1964) is important in predicting water levels and currents especially within the surf zone area (Dietrich et al. 2011).

2.2 Model domain

The model domain covers the Gulf of Maine and adjacent waters surrounding Cape Cod, Nantucket Sound, Buzzards Bay, and Nova Scotia (for simplicity, this area is referred to as the Gulf of Maine). The water depth ranges from about 4000 m in the deep ocean to less than 1 m in the coastal area. An unstructured mesh was created with 170,970 nodes and 317,992 triangular elements. The grid resolution ranges from 25,000 m along the offshore boundary to 15 m in the coastal area in order to locally resolve the bathymetry and complicated geometry of coastline. Figure 3 shows the model coverage and the unstructured mesh. The detailed information of wave buoys and tide gauges within the model domain is listed in Table 1 and Table 2, respectively.

The model domain was selected based on previous and present domain and grid sensitivity studies of SWAN + ADCIRC for severe storms. For example, the hurricane storm surge study by Blain et al. (1994) indicates that the domain with deep Atlantic Ocean boundaries minimizes the influence of boundary conditions. Chen et al. (2013) and Beardsley et al. (2013) also selected a domain with boundaries well off continental shelf break for coastal inundation simulation in the Gulf of Maine. Nevertheless, the 2-D depth integrated (2DDI) model of ADCIRC is likely to not properly resolve the current in deep ocean where the vertical variation of the current becomes important.

2.3 Surface wind and pressure forcing

The authors compared two sets of wind for wave and surge simulation in the Gulf of Maine, the NASA Cross-Calibrated Multi-Platform (CCMP) ocean surface wind (http://rda.ucar.edu/datasets/ds745.1) and NCEP North American Regional Analysis (NARR) wind data (http://rda.ucar.edu/datasets/ds608.0). The 6-hourly CCMP wind covers globally with 0.25° grid resolution, while the 3-hourly NARR wind covers Continental USA with 32 km (approximately 0.30°) grid resolution. We found that the NARR wind performed better compared with the CCMP wind in terms of simulation results for the Patriot's Day storm. In this paper, simulation results driven by NCEP North American Regional Reanalysis (NARR) database are presented. This database is generated using the high resolution 32 km NCEP Eta Model

Table 1 Wave buoys in the Gulf of Maine

Wave buoy	Buoy location	Water depth/m
44005	Gulf of Maine, 78 NM East of Portsmouth, NH	206.0
44008	Nantucket, 54NM Southeast of Nantucket	66.4
44011	Georges Bank, 170 NM East of Hyannis, MA	82.9
44017	Montauk Point, 23 NM SSW of Montauk Point, NY	52.4
44018	Cape Cod, 24 NM East of Provincetown, MA	217.6
44024	Northeast Channel	225.0
44030	Western Maine Shelf	62.0
44032	Central Maine Shelf	100.0
44033	West Penobscot Bay	110.0
44034	Eastern Maine Shelf	100.0

with 45 vertical layers output together with the Regional Data Assimilation System. By incorporating regional data assimilation in the North America, the dataset has better accuracy of temperature, winds, and precipitation than other datasets available in this area. It outputs wind, air pressure, precipitation, and other meteorological parameters every 3 hours at 29 vertical levels.

Wind field at 10 m above sea surface and sea surface pressure were used as meteorological forcing for the ADCIRC and SWAN model. Figure 4 shows the comparison of wind vectors at 10 m above sea surface at four wave buoys in the Gulf of Maine. It can be seen that the magnitude and direction of NARR wind output agree reasonably well with buoy measurements, which provides confidence for wave and surge modeling.

2.4 Model setup and implementation

The 2-D depth integrated version of ADCICR (ADCIRC-2DDI) was used for tide and storm surge prediction. The finite amplitude and convection terms were activated. Lateral viscosity was set with a constant of 5 m^2/s following Yang and Myers (2008) and Bunya et al. (2010) through the whole domain. The air-sea drag coefficient defined by Garratt's drag formula (Garratt 1977) was used with a cap of $C_d \leq 0.0035$. The drag coefficient formula of Garratt (1977) is consistent with the relation proposed by Charnock (1955) between aerodynamic roughness length (z_0) and friction velocity (u_*), viz., $z_0 = \alpha u_*^2/g$ when $\alpha = 0.0144$ over the ocean. Garratt (1977) approximated Charnock's relation (1955) based on previous observations of wind stress and wind profiles over the ocean using a neutral drag coefficient (referred to 10 m) for a 10-m wind speed ranging between 4 and 21 m/s. The drag coefficient of Garratt (1977) was still widely used for the most recent work on storm surge modeling in literature, e.g., Westerink et al. (2008), Bunya et al. (2010) and Dietrich et al. (2010).

The hybrid friction relationship is used to specify a spatial varying bottom friction coefficient depending on water depth (Luettich and Westerink 2006),

$$C_f = C_{f\min}\left[1 + \left(\frac{H_{\text{break}}}{H}\right)^{\theta_f}\right]^{\gamma_f/\theta_f} \quad (1)$$

When the water depth is larger than H_{break}, a constant friction coefficient $C_{f\min}$ based on standard Chezy friction law is applied; when the water depth is less than H_{break}, the Manning type friction law is applied where the friction coefficient increases with decreasing water depth, which is more realistic in shallow water areas. The parameters $C_{f\min} = 0.03$, $H_{\text{break}} = 2.0m$, $\theta_f = 10$, and $\gamma_f = 1.33333$ were used as recommended by Luettich and Westerink (2006).

The eight most significant astronomical tide constituents (M2, S2, N2, K2, K1, P1, O1, and Q1) were used to drive the model along the open boundary. The corresponding harmonic constants of the eight tidal constituents were interpolated from the global model of ocean tides TPXO (http://volkov.oce.orst.edu/tides/global.html). The time step for ADCIRC was set to 1 s to maintain computational stability.

The wave model SWAN shares the same unstructured mesh and surface wind forcing with ADCIRC. The 2-D wave spectra output by SWAN hindcast in the Western North Atlantic Ocean was used as the offshore boundary conditions, to allow swells generated outside of the model domain to propagate reasonably into the model domain.

Table 2 Tide gauges in the Gulf of Maine

Tide gauge	Location	Water depth/m
8413320	Bar Harbor, ME	6.0
8418150	Portland, ME	12.0
8423898	Fort Point, NH	9.0
8447930	Woods Hole, MA	5.0

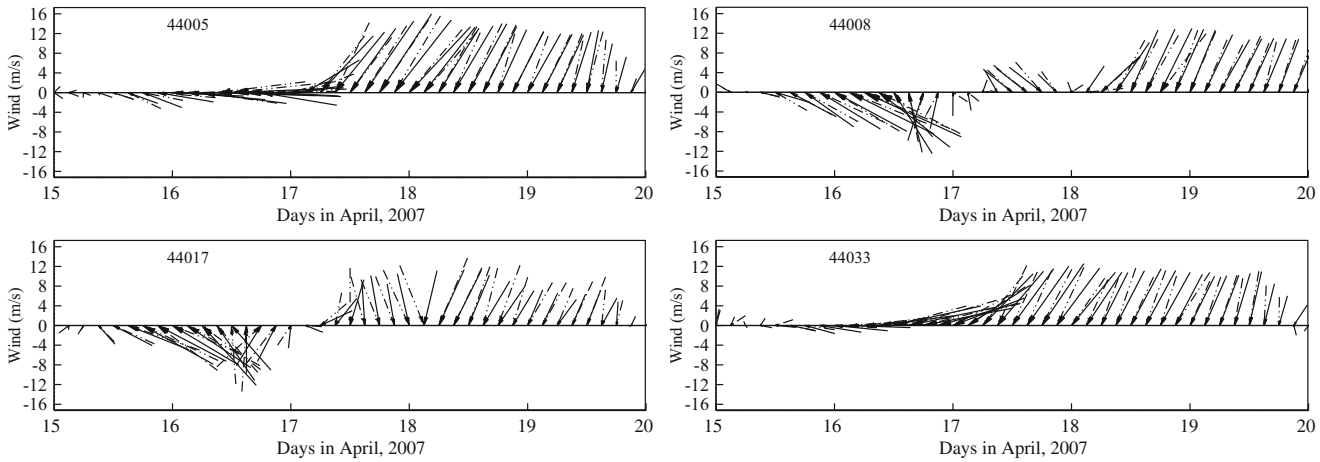

Fig. 4 Comparison of NARR winds with buoy measurements at buoy 44005, 44008, 44017 and 44033: Observed data (*black dash-dotted vector*); NARR reanalysis wind output at buoy stations (*black solid vector*)

The prescribed spectrum frequencies range from 0.031384 to 1.420416 Hz and are discretized into 40 bins on a logarithmic scale. The wave spectrum is solved in full circle with a directional resolution of 10°. The JONSWAP formulation (Hasselmann et al. 1973) was used for bottom friction. The friction coefficient of $0.038 m^2 s^{-3}$ was used for both wind waves and swell (Zijlema et al. 2012). The time step for integration is set to 600 s.

The coupling interval of the ADCIRC and SWAN models is the same as the time step for SWAN. ADCIRC will pass wind forcing, water level, and currents to SWAN every 600 s, while SWAN passes radiation stress to ADCIRC to update the calculation. The model ran for 30 days from 4/1/2007 to 4/30/2007 from cold start. The elevation-specified boundary condition was first ramped up for 5 days with a hyperbolic tangent function until an equilibrium state was reached before surface wind and pressure forcing were applied.

Three cases were run: (1) tide-surge predictions without wave effects, (2) wave prediction without temporal varying water level and currents, (3) a fully coupled SWAN + ADCIRC run to include tide-surge and wave interaction.

3 Model validation

The model prediction of water level, depth-averaged current, and wave parameters were validated hourly during the storm period. The tide and surge levels were validated at four coastal tide gauges. The depth-averaged current was validated by the vertical current profiles measured by Acoustic Doppler Current Profilers (ADCP) at two buoy sites. The significant wave height and dominant wave period were validated at four wave buoys over the continental shelf and within coastal bays. The following statistical parameters are used to quantify model-data comparisons:

(i) Mean Bias, the difference between the mean of observed data and model result;
(ii) Peak Bias, the difference between the observed data and model result at the storm peak;
(iii) RMSE, the root mean square error to evaluate the average accuracy of model prediction over the duration of the storm.

3.1 Tide and surge

The predicted astronomical tide during the modeling period was first compared with data from NOAA/CO-OPS tide gauges, which is a prerequisite since coastal flooding often happens at or near high tide especially at high latitudes (Wolf 2009). The water level recorded by NOAA/CO-OPS tide gauges was analyzed using the MATLAB harmonic analysis toolbox T-Tide (Pawlowicz et al. 2002) to separate tidal components and residuals. The extracted tidal level was then compared with model predictions. Figure 5 shows the comparison result at four tide gauges along the coast of the Gulf of Maine, including gauge 8413320 (Bar Harbor, Maine), 8418150 (Portland, Maine), 8423898 (Fort Point, New Hampshire) and 8447930 (Woods Hole, Massachusetts) from north to south. Table 3 summarizes the validation metrics. The model prediction agrees well with measurement both in magnitude and phase. The observed tidal level at high tide is slightly under-predicted except at tide gauge 8447930, possibly due to the overestimated bottom dissipation and numerical diffusion accumulated with time.

Figure 6 shows the comparisons of predicted surge levels with measurements at the same four tide gauges. Since the wave effect on surge level is negligible at these four tide gauges, only surge level due to direct meteorological forcing was plotted in Fig. 6 to compare with recorded residuals by the tide gauges. The wave effect on surge level at these four tide

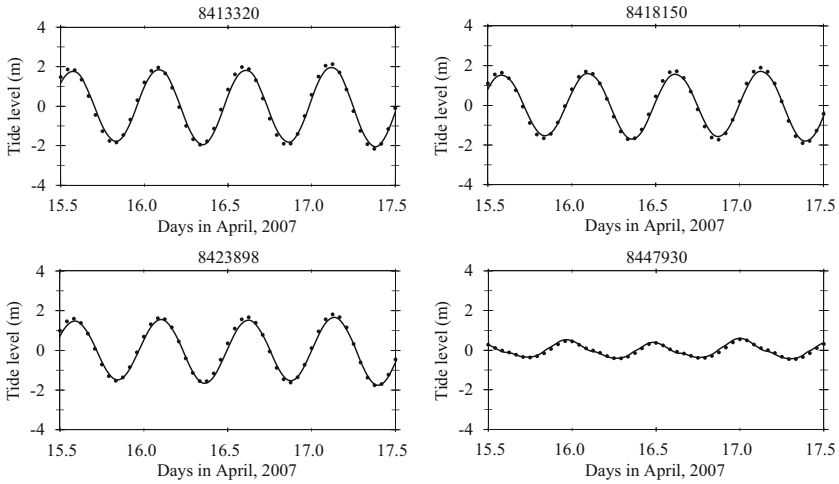

Fig. 5 Comparison of predicted astronomical tides with measurements. Measurement (*black dots*); model prediction (*black solid line*)

gauges is negligible mainly because these gauges are located in estuaries sheltered from offshore storms. However, wave contribution to surge level can be significant in shallow open coast (Brown et al. 2013).

The measured surge by tide gauges was reasonably predicted. Strong tidal modulation of surge can be identified at tide gauge 8413320, 8418150, and 8423898, where tidal range is over 4.0 m. While the first peak of surge level was well reproduced, the second peak was underestimated by approximately 0.2 m. This deficit is due to the following reasons: (1) The Ekman transport (Sverdrup et al. 1942) becomes important as the wind direction changed from southeast to east when the storm gradually moved to the east from April 17 to April 18 (Figs. 1 and 2). When the wind veered to the east, the surface wind stress produced Ekman transport along the offshore boundary of model domain, which contributes to elevated water level along the coastline at the second storm peak; (2) The elevated water level along the lateral boundary at Scotian Shelf (Fig. 3a) is not negligible. In the present model, only tidal constituents were specified along the ocean boundary, while the effect of elevated water level by surge at the lateral boundary and Ekman transport at the offshore boundary were both neglected. This deficit may be minimized by either extending the model domain so the model results are less sensitive to offshore and lateral boundary conditions or applying more realistic boundary conditions, e.g., current velocity and water level (e.g. Blain et al. 1994). In this study, we will focus on tide-surge and wave interaction during the tidal cycle containing the first storm peak when the model predictions compare well with measurements (Tables 4, 5 and 6).

3.2 Currents

The total current driven by tide, direct meteorological forcing, and wave was validated in this section. The vertical current profile by ADCP at two buoy sites, buoy 44024 and buoy 44033, was integrated to obtain depth-averaged current and compare with model prediction.

The ADCP measurements of depth-averaged current at the wave buoys are in good agreement with model prediction (Fig. 7). Currents at these two buoys are mainly driven by the tide. The east component of the current, U, at both buoy sites was slightly overpredicted. The wave effect on the depth-averaged current at the two buoy sites is negligible since the water depth at these two buoy sites is in the order of 100 m, where the wave radiation stress is small. However, along the shallow open coast where considerable wave transformation and dissipation take place, wave effect on current can be significant. ADCIRC currently only include wave radiation stress in the wave-current interaction but not stokes drift. It also neglects the wave-current interaction through surface stress and bottom stress.

3.3 Waves

Wave predictions with and without tide-surge and wave interactions are compared with measurements in Fig. 8. Wave growth and decay before and after the storm are well predicted. The prediction with and without wave-current interaction is similar to each other at the four wave buoys, indicating that wave-current interaction at these buoys is negligible. Since these buoys are located in relatively deep water where the

Table 3 Error in model prediction of observed tidal level by tide gauges

Tide gauge	Mean bias (m)	RMSE (m)
8413320	0.011	0.182
8418150	0.018	0.148
8423898	0.055	0.128
8447930	-0.029	0.063

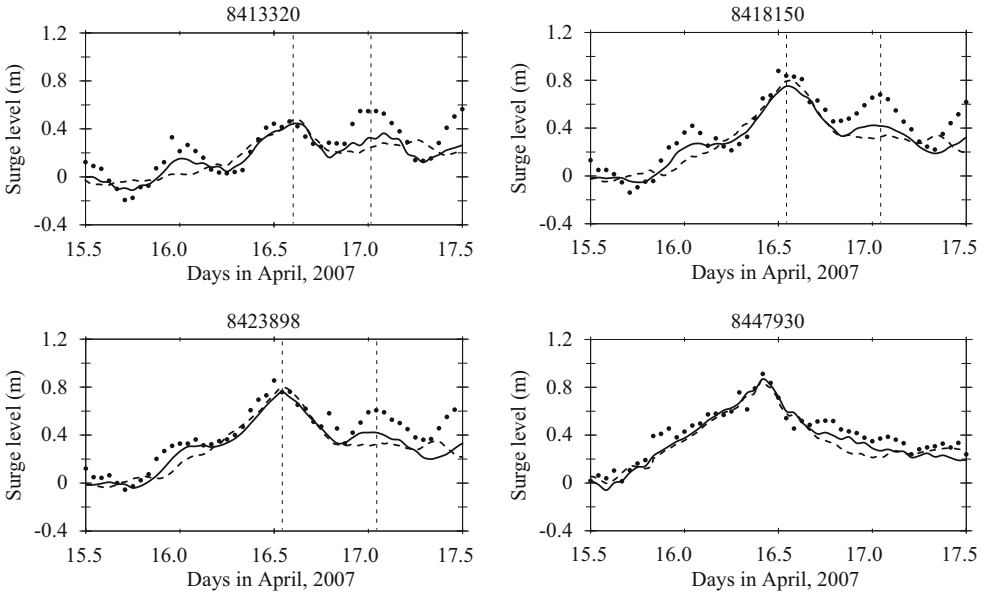

Fig. 6 Predicted storm surge in comparison with measurements. Measurements (*black dots*), model prediction with (*black solid line*), and without (*black dash line*) tide-surge and wave interaction. The two peaks of storm surge are marked by vertical *dash lines*

local current is small (see Table 1 for the water depth for all buoys), negligible current effect on waves is expected. This may not be the case at other locations, where the current is large, e.g., over Georges Bank where detailed analysis of current effect on directional wave spectra is carried out in Section 4. While the peak of significant wave height was captured well by the model, the wave height after storm peak was underestimated. The rapid evolution of the storm after April 17 (Figs. 1 and 2) generated fast transient wind. The NOAA NARR reanalysis wind with 3-hourly interval cannot capture the rapid variations of wind. In general, it is expected that higher resolution wind at higher sampling rate will likely improve the model prediction (e.g. Zou et al. 2013).

4 Model results

In this section, analysis of tide-surge and wave interaction on circulation and wave was carried out by comparing the wave and circulation at the peak of the storm (1400UTC April 16, 2007) for different scenarios. The wave setup and wave-induced current in Saco Bay over the tidal cycle at the peak of the storm was also analyzed.

4.1 Wave effects on circulation

Figure 9 shows the depth-averaged velocity in the Gulf of Maine at the storm peak. The depth-averaged velocity is relatively large in the Bay of Fundy and over Georges Bank. The maximum current speed is identified within the Bay of Fundy and reaches 2.0 m/s. At the southern flank of the Georges Bank, the depth-averaged current ranges from 0.6 m/s to 1.0 m/s. At the northern flank, the tidal current speed is slightly larger, between 0.8 and 1.2 m/s. At locations over the Georges Bank with minimum water depth, the depth-averaged current speed reaches 1.4 m/s. The predicted circulation pattern in shallow water region of the Gulf of Maine by the present 2-D model in Fig. 9 agrees reasonably well with the numerical results by Greenberg (1983) and Xue et al. (2000) and field observations by Pettigrew et al. (2005).

By comparing Fig. 9a, b , the effect of wave-current interaction on circulation is most significant over Georges Bank. Over the bank, the depth-averaged velocity is increased by approximately 0.2 m/s by the presence of wave through wave radiation stress, which is mainly due to the shallow water depth. The Georges Bank dissipates significant amount of wave energy through bottom friction and breaking, which leads to a decrease in wave height, therefore, wave radiation stress. The wave radiation stress is proportional to the square of wave height. The corresponding excessive momentum flux on the circulation generates the wave-induced circulation in Fig. 9c.

Since the wave radiation stress gradient becomes significant mainly in coastal areas where wave height changes drastically due to shallow water wave processes such as wave refraction, wave diffraction, bottom friction effect, and wave

Table 4 Error in model prediction of observed surge level by tide gauges

Tide gauge	Mean bias (m)	Peak bias (m)	RMSE (m)
8413320	0.066	0.029	0.116
8418150	0.085	0.175	0.124
8423898	0.095	0.145	0.127
8447930	0.051	0.020	0.080

Table 5 Error in model prediction of observed current by ADCP

ADCP	Without tide-surge and wave interaction				With tide-surge and wave interaction			
	U component		V component		U component		V component	
	Mean bias (m)	RMSE (m)	Mean bias (m)	RMSE (m)	Mean bias (m)	RMSE (m)	Mean bias (m)	RMSE (m)
44024	-0.022	0.161	-0.091	0.154	-0.016	0.176	-0.103	0.172
44033	-0.034	0.052	0.003	0.109	-0.051	0.067	0.051	0.136

Table 6 Errors in model prediction of observed significant wave height by wave buoys

Wave buoy	Without tide-surge and wave interaction			With tide-surge and wave interaction		
	Mean bias (m)	Peak bias (m)	RMSE (m)	Mean bias (m)	Peak bias (m)	RMSE (m)
44030	0.561	0.580	0.798	0.583	0.499	0.811
44032	0.314	0.425	0.609	0.369	0.319	0.655
44033	−0.419	−0.763	0.685	−0.490	−1.147	0.801
44034	0.283	1.074	0.558	0.341	1.200	0.605

breaking, its contribution to circulation is more evident in these areas. The Saco Bay was selected to illustrate the wave effect on water level and circulation during the storm. The low-lying coast of this area is prone to flooding due to the

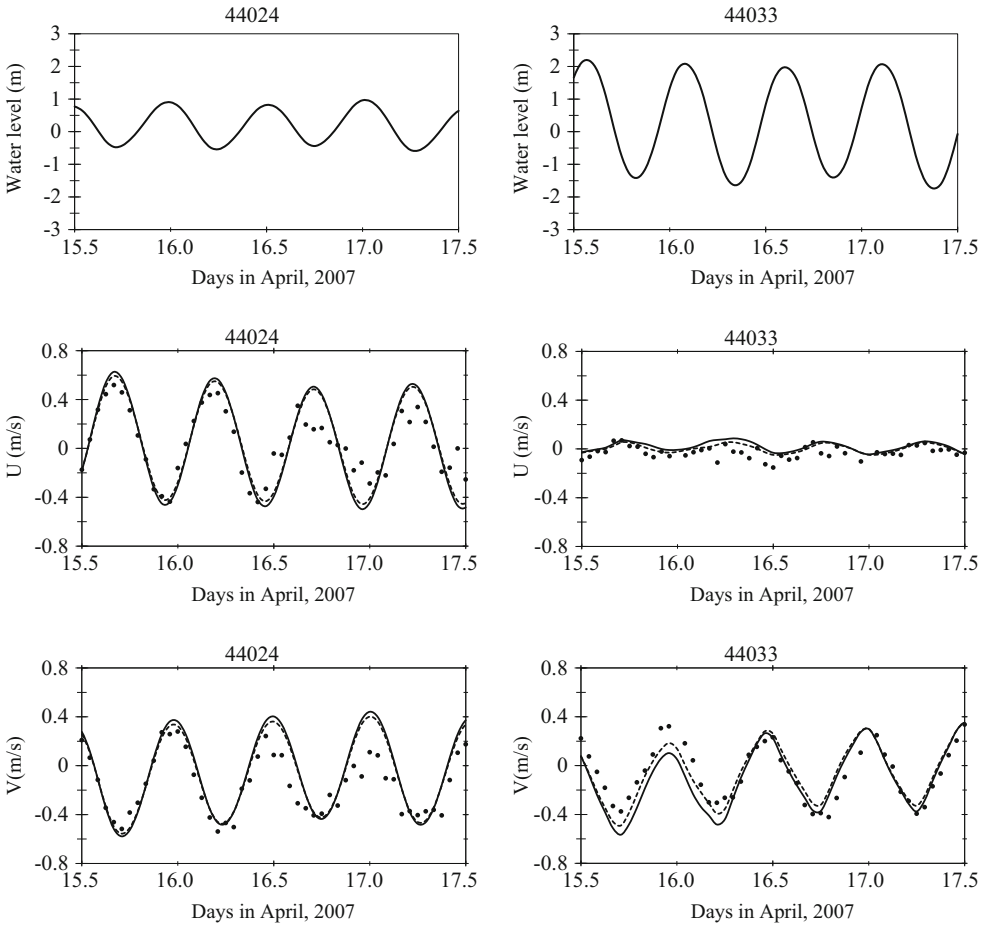

Fig. 7 The predicted water level (*upper*) and the comparisons of the predicted depth-averaged current velocity in the east, U, (*middle*) and north direction, V, (*lower*) with the ADCP measurements. ADCP measurements (*black dots*); model prediction with wave-current interaction (*black solid line*); model prediction without wave-current interaction (*black dash line*)

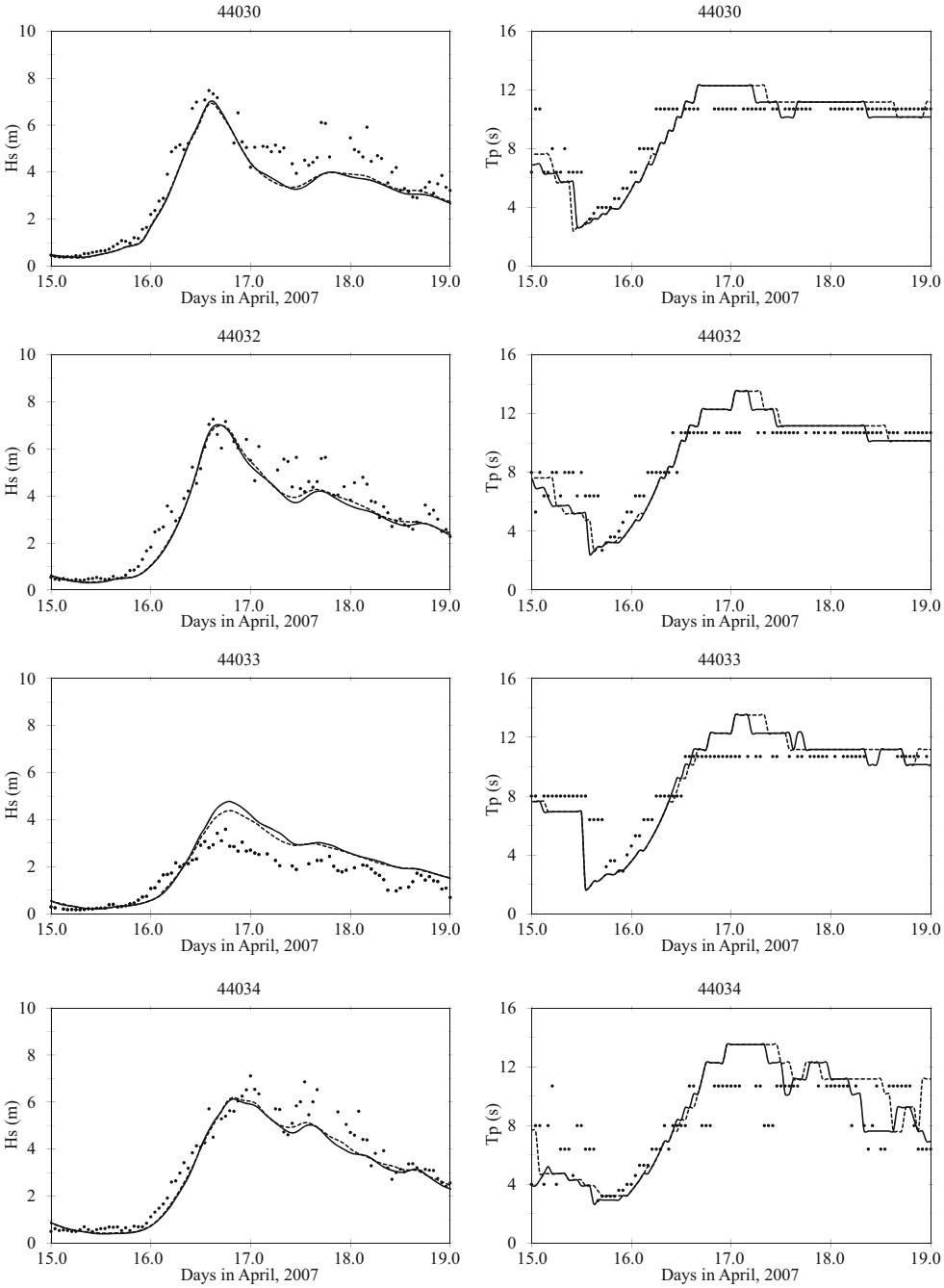

Fig. 8 Comparisons of predicted wave parameters with buoy measurements. Significant wave height (*left*) and dominant wave period (*right*). Wave buoy data (*black dots*); model prediction with (*black solid line*) and without (*black dash line*) wavecurrent interaction

combined effect of elevated water level and large waves during storm events. The coastal dynamics and sediment transport in the bay have been examined using observation data in several studies (e.g. Hill et al. 2004; Kelley et al. 2005; Brother et al. 2008; Tilburg et al. 2011); however, no previous study has focused on tide-surge and waves in response to storms in the bay using numerical modeling. Figure 10 shows the bathymetry of the Saco Bay. The time series of wave parameters, tidal level, surge level and wave setup was output at point A in Fig. 10 where the water depth is 3.5 m.

Figure 11c shows the wave field at the peak of the storm in the Saco Bay. It can be seen that the contour of the significant wave height is in parallel with the depth contour in Fig. 10 due to wave refraction. As the wave propagates towards the shore, wave height increases due to the shoaling effect and decreases due to directional spreading, bottom friction, and wave breaking, which generate excess momentum flux, i.e., wave radiation stress. The wave radiation stress exerts on the mean flow and generates wave setup and wave-induced current. Figure 11d shows the radiation stress gradients. The radiation

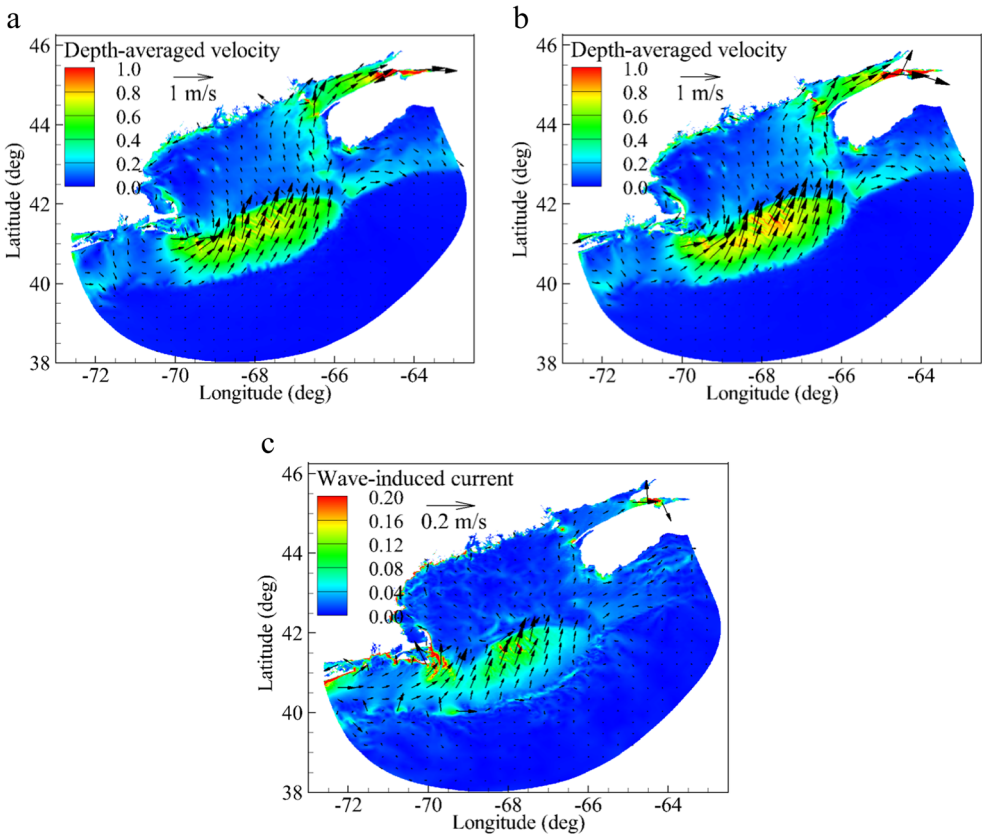

Fig. 9 Depth-averaged velocity at the peak of the storm (1400UTC April 16, 2007). **a** Without wave effect. **b** With wave effect. **c** Wave-induced current

stress gradients are relatively large where bottom topography changes abruptly. Along the central part of the coast in this area, the radiation stress gradients are generally normal towards the coastline and reaches maximum when significant wave height changes most. While at both the northern end and southern end of the coast, the radiation stress gradients are in an oblique angle with the coastline, exerting longshore stress on the circulation. The magnitude of radiation stress gradients ranges from 0.0024 to 0.0060 N/m^2 along the coastline.

Figure 11a, b shows the surface elevation and depth-averaged velocity with and without wave effect at the peak of the storm. It can be seen that the surface elevation is increased by 0.2 m along the coast due to wave setup, which accounts for 20 % of the total surge level. The maximum wave setup is at the river mouth of the Saco River. The depth-averaged velocity is also significantly enhanced by the presence of wave. Wave-induced current is dominant in the bay and reaches over 1.0 m/s, which is in the same order as measured by Hill et al. (2004). A clockwise circulation gyre is identified at the offshore of the Saco River. When tide-surge and wave interaction is considered, the gyre is greatly enhanced and moved further offshore (Fig. 11b). Along the central part of the coast, the southward and northward longshore current converges and produces a strong current in the offshore direction due to mass conservation in the same fashion as rip current. The offshore current further veers to the south. Part of the southward current continues to the south while the rest merges into the clockwise circulation. The wave-induced circulation in the Saco bay is a major driving force for

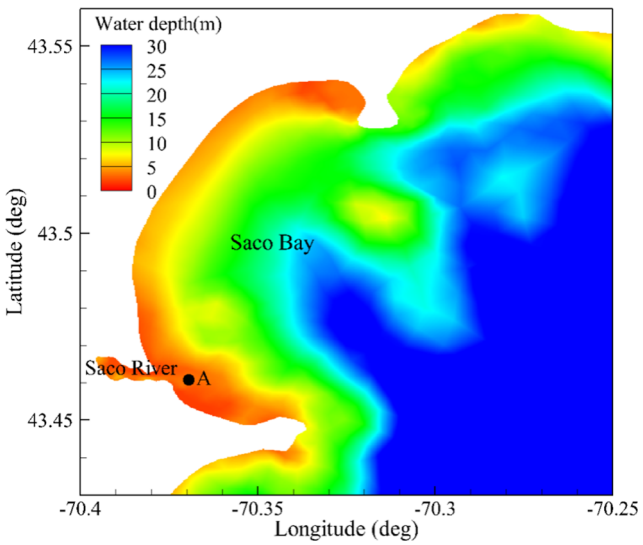

Fig. 10 Bathymetry of the Saco Bay. Time series of water level and current predicted by the present model in Fig. 12 is the output at point A denoted by the *black circle* here

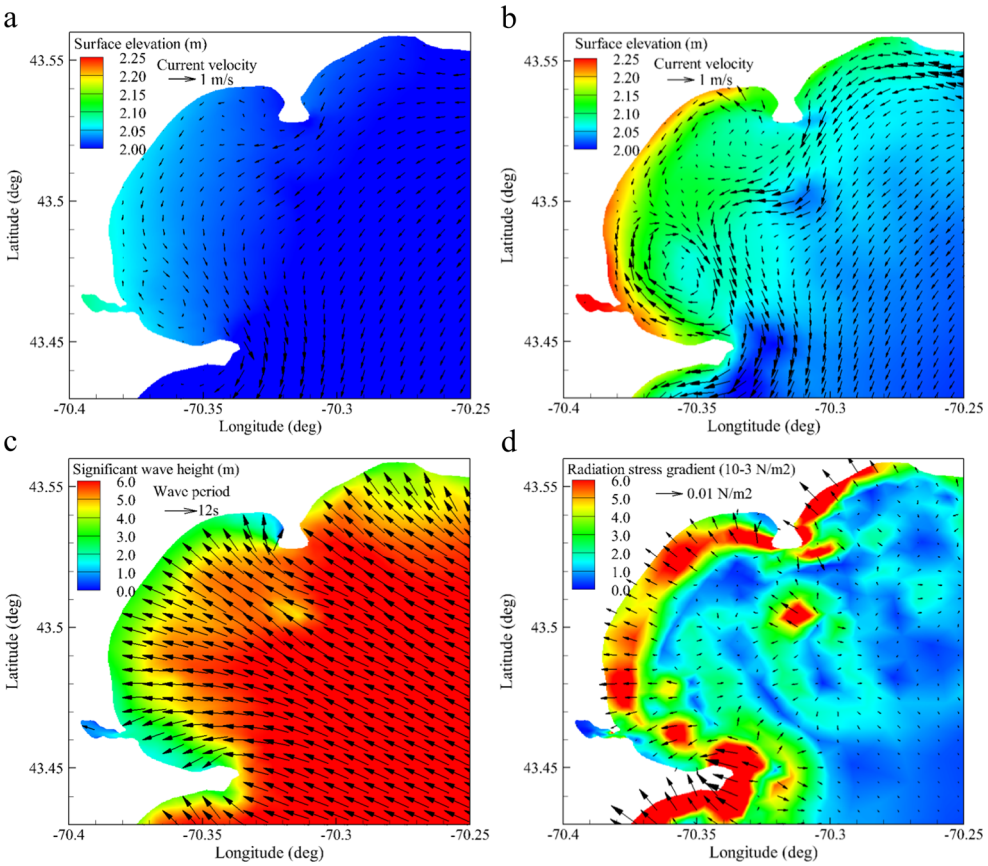

Fig. 11 Snapshot of circulation and wave field in Saco Bay at 1400UTC April 16, 2007. **a** Circulation without wave effect. **b** Circulation with wave effect. **c** Wave field. **d** Radiation stress gradients

the sediment transport and beach erosion and accretion in the bay.

The time series of predicted tidal level, surge level, significant wave height and wave setup at point A were plotted in Fig. 12 to further analyze the effect of tide-surge and wave interaction. At point A, while the maximum surge level of 0.9 m occurs 2 h before the high tide, the maximum wave setup coincides with high tide as well as maximum significant wave height. Wave setup is mainly related to wave radiation stress gradients in the cross-shore direction. At the coast, tide plays a significant role in modulating wave height (Zou et al. 2013). The wave height is dependent on water depth due to wave shoaling, refraction, and breaking. At high tide, excess momentum flux is generated by wave transformation and breaking in the cross-shore direction and results in elevated water level through wave setup. As tidal level falls, the significant wave height decreases and wave setup decreases correspondingly.

Both wave setup and wave-induced currents in Saco Bay at the four tidal phases illustrated in Fig. 12 were shown in Fig. 13. As tidal level increases, significant wave height and wave setup increases and reaches their maxima at high tide. Two clockwise circulation gyres are formed and located close to the headlands to the north and south of Saco Bay. The two gyres sustained for 26 h during the storm. Wave energy converges at the headlands and diverges in the bay, which generates large momentum fluxes from the headlands to the inner bay and forms the gyres. The two gyres are also intensified as tidal level increases.

4.2 The impact of tide-surge on waves

The analysis of tide-surge and wave interaction on wave prediction is carried out in this section. It is evident from Fig. 14 that wave distribution within the model domain is similar with and without tide-surge and wave interaction. The storm-generated significant wave height exceeded 7.0 m over the majority of the model domain at the storm peak. The impact of tide-surge and the associated current on waves is significant over Georges Bank (the square box in Fig. 14). Over the bank, the significant wave height is decreased by 0.3~0.5 m mainly due to current effect. While the tidal range over the bank is relatively small comparing with the water depth, increasing from 1.0 m at the southern flank to 2.0 m at the northern flank, the current has a magnitude of 1.0 m/s. At the storm peak, the current flows towards the northeast and is normal to the mean wave direction, it slightly refracts waves.

2-D directional wave variance density spectra at four wave buoys (buoy 44005, 44008, 44011, and 44018) were further analyzed to assess the contribution of tide-surge and the associated current to waves. Buoy 44008 and 44011 are located at the southern flank of Georges Bank and buoy 44005 and

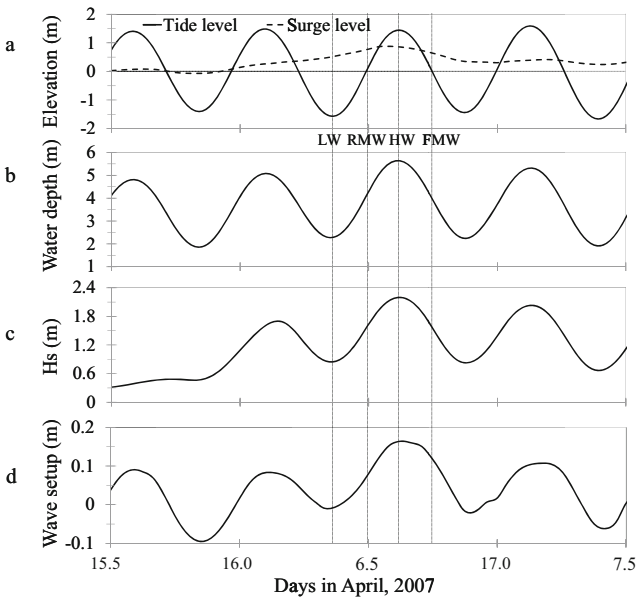

Fig. 12 Time series of modeled elevation, significant wave height and wave setup at point A in Saco bay indicated in Fig. 7. The *four vertical dash lines* denote the four tidal phases, in which LW is for low water, RMW is for rising mid-water, HW is for high water and FMW is for falling mid-water, respectively

44018 are located at the inner Gulf of Maine (Fig. 3a). Current has a significant impact on wave energy redistribution over frequency and directional domain. The frequency range of wave spectra is generally extended to higher frequencies by considering tide-surge and wave interaction, which can be explained by Doppler shift of wave frequency in the presence of current. At buoy 44005, while wave variance density remain the same at peak wave frequency, it decreases from the east and increases from the south with tide-surge effect. The peak wave variance density is significantly reduced by the tide and surge current at buoy 44008, 44011, and 44018. At the two buoys located at the southern flank of the Georges Bank, buoy 44008 and 44011, the reduction of peak wave variance density is largest. Over the Georges Bank, the depth-averaged current speed reaches 1.2 m/s and strong current shear is present, which alter the direction and frequency distribution of wave energy (Fig. 15).

The impact of tide-surge and the associated current on waves at the storm peak in the Saco Bay is shown in Fig. 16. While wave distribution is similar with and without tide and surge effect, the significant wave height near the coast is increased by 0.8~1.0 m with the presence of the tide-surge.

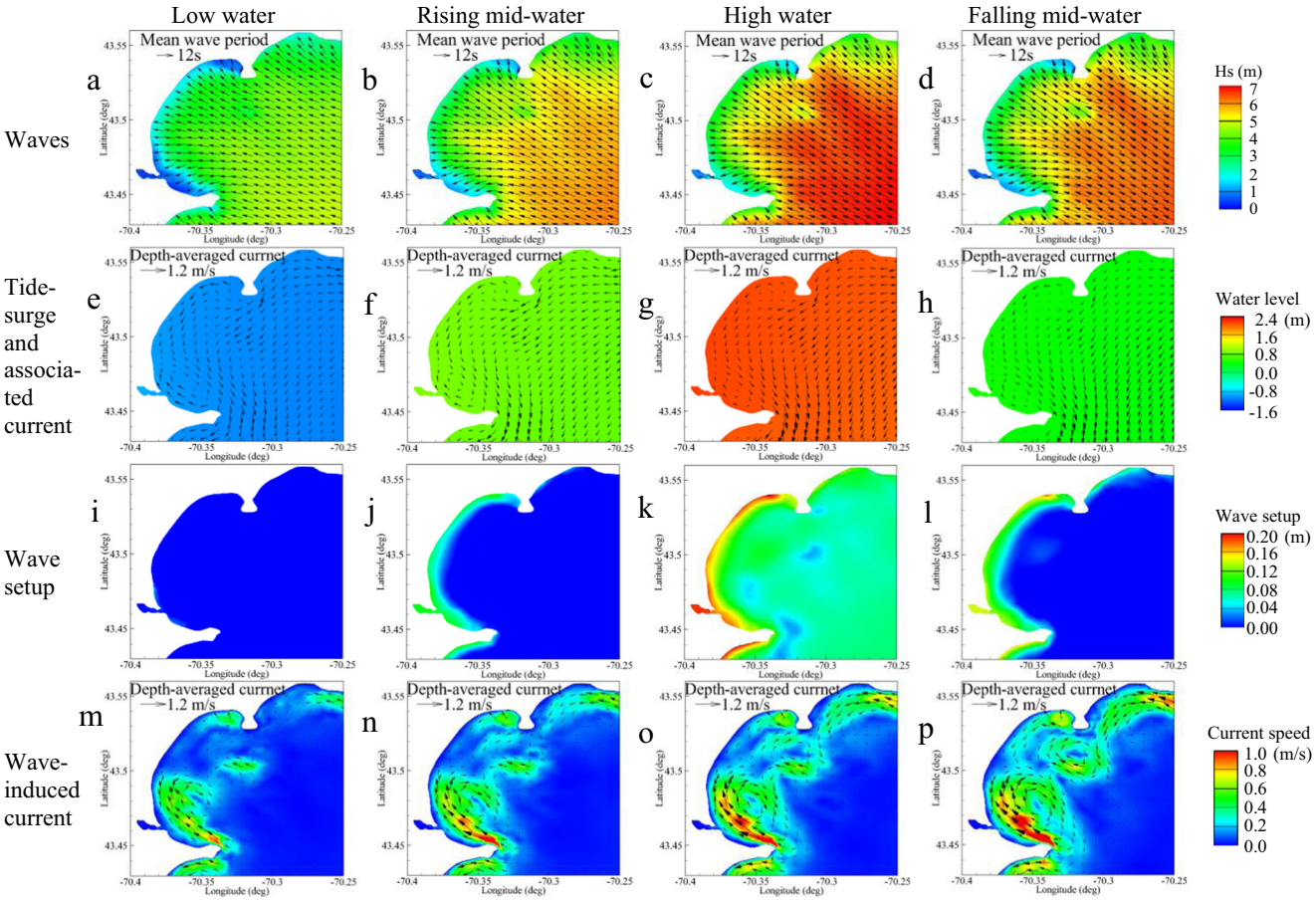

Fig. 13 The wave fields (*top panel*), the tide-surge level and associated current (*the second panel*), the wave setup (*the third panel*), and wave-induced current (*the bottom panel*) in Saco Bay at the four tidal phases marked in Fig. 10

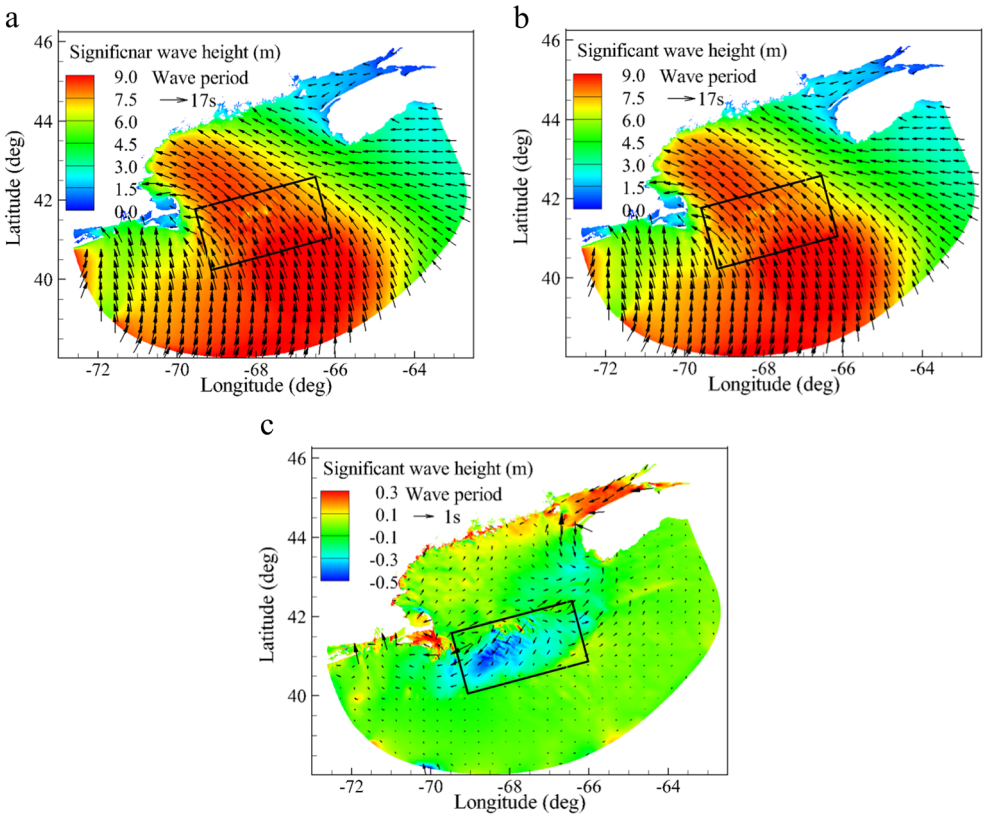

Fig. 14 Wave fields at 1400UTC April 16, 2007. **a** Without tide-surge effect. **b** With tide-surge effect. **c** With minus without tide-surge effect, in which the *red color* indicates the increase of wave height by tide-surge effect while the *blue color* indicates the decrease of wave height

For example, the 5-m contour line of significant wave height moves further towards the coastline due to the tide-surge effect. The mean tidal range in Saco Bay is 2.7 m. The peak surge level of 0.8 m occurred 2 h before high tide. The elevated water level significantly increases water depth in Saco Bay. Towards the coast, wave propagation and transformation is dictated by water depth and wave height contours are parallel with depth contours. Figure 16c indicates that waves slightly converge from the northern and southern end of Saco Bay towards its mid-coast due to current refraction.

5 Conclusions and discussions

The fully coupled spectral wave and circulation model SWAN + ADCIRC was applied to investigate tide-surge and wave interaction in the Gulf of Maine during an extratropical storm, the 2007 Patriot's Day storm, which retrograded towards the coastline and caused significant coastal flooding and severe beach erosion along the New England coast.

In the Gulf of Maine, tide-surge and wave interaction is significant over Georges Bank and in the coastal areas. During the 2007 Patriot's Day storm, over Georges Bank, the wind-induced current was approximately 0.2 m/s, accounting for 17 % of total current at the storm peak. The wave-induced current mainly occurs at the shallow bathymetry over the bank, where the wave energy was dissipated significantly by bottom friction and generated momentum flux exerting on the mean flow in the cross-bank direction. Within Saco Bay, the circulation was dominated by wave-induced current during the storm. The magnitude of wave-induced current reached 1.0 m/s, comparable with previous studies. Two clockwise circulation gyres formed in the bay, mainly driven by waves and due to the shallow water bathymetry and configuration of the coastline. When waves entered Saco Bay, wave energy converged at the headlands at the northern and southern end of the bay and diverged at the inner bay, generating a radiation stress gradient that drives a longshore current from both ends to the inner bay coast. These longshore currents converged and fed into a current directed away from shore at the mid-coast of Saco Bay. To our knowledge, wave-induced currents over Georges Bank and in the Saco bay have not been studied previously.

Wave setup at the storm peak was 0.2 m along the coast of Saco Bay and reached its maximum at the mouth of the Saco River. Both wave setup and wave-induced current were significantly modulated by the tide in Saco Bay. During the tidal cycle containing the storm peak, wave setup increased with tidal level and the maximum wave setup coincided with the high tide. The clockwise circulation gyres were also intensified at high tide. At the coast, wave transformation is mainly dependent on water depth. At high tide, the wave height

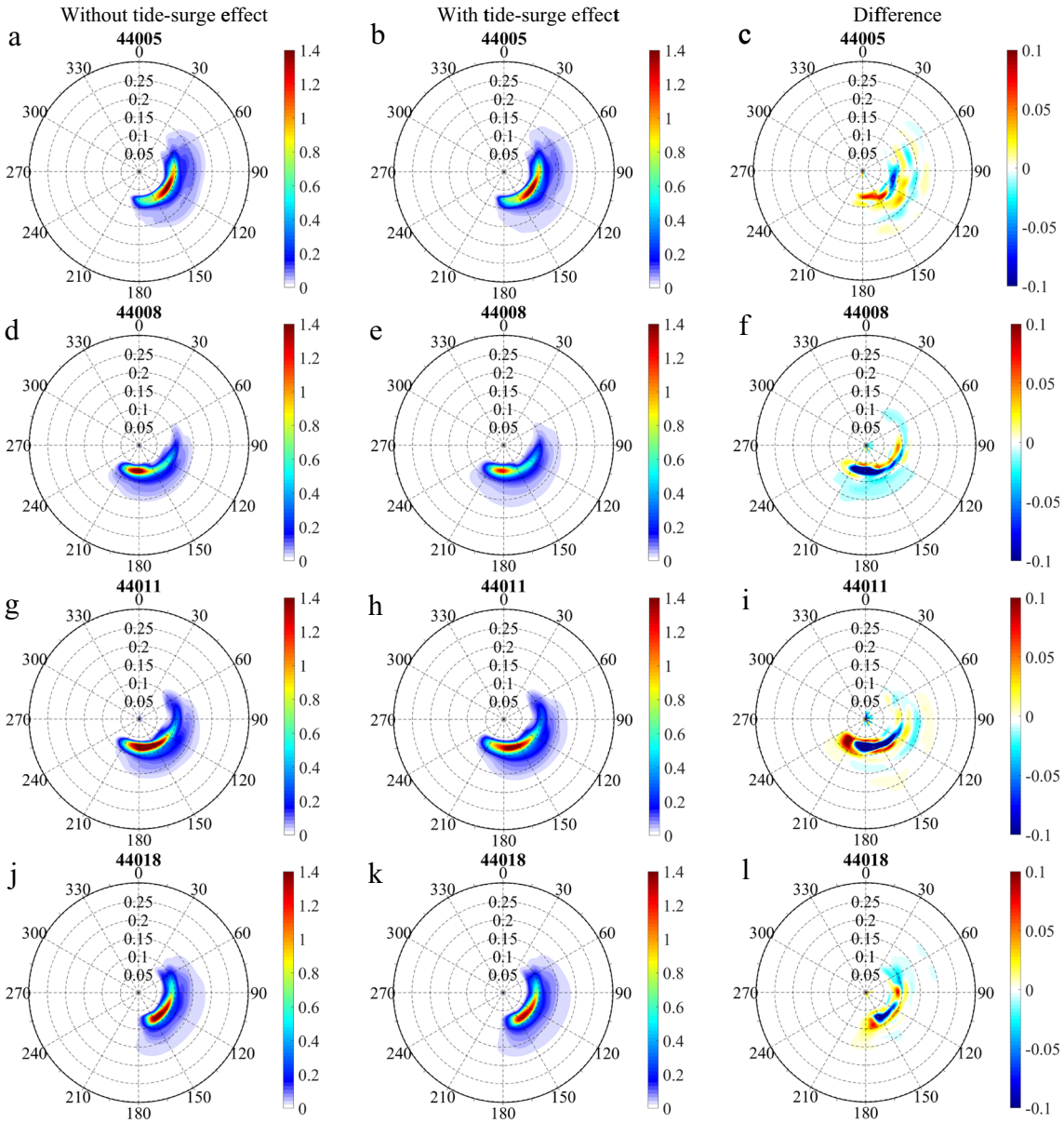

Fig. 15 Directional wave variance density spectra at four wave buoys 44005, 44008, 44011 and 44018. The unit of the variance density is m^2/Hz/deg. **a**, **d**, **g**, **j** without tide-surge effect. **b**, **e**, **h**, **k** with tide-surge effect. **c**, **f**, **i**, **l** With *minus* without tide-surge effect

gradient reached its maximum, as did the wave radiation stress gradient in the cross-shore direction, producing the maximum wave setup.

The wave prediction was improved significantly by including the tide-surge effect in these two regions. Over Georges Bank, the significant wave height was decreased by 0.3~0.5 m due to wave refraction by current over the bank. Wave height in Saco Bay was modulated by the tide along the coast and it increased with tidal level. The predicted directional wave spectra at the four wave buoy locations in the Gulf of Maine indicate that wave energy is shifted to higher frequencies by the tide-surge interaction, however, the current had negligible effect on the directional distribution of spectral wave energy at these locations.

In the coupled SWAN + ADCIRC model, ADCIRC calculates water level and depth-averaged currents and pass them to SWAN, SWAN then computes the radiation stress gradients and passes them to ADCIRC (Dietrich et al. 2011). The 2-D depth uniform wave radiation stress formula proposed by Longuet-Higgins and Stewart (1962, 1964) used here is proportional to the square of wave height. The response of the flow to the wave radiation stresses tends to increase with decreasing water depth (Longuet-Higgins and Stewart 1962). Since wave radiation stress gradient is only significant where

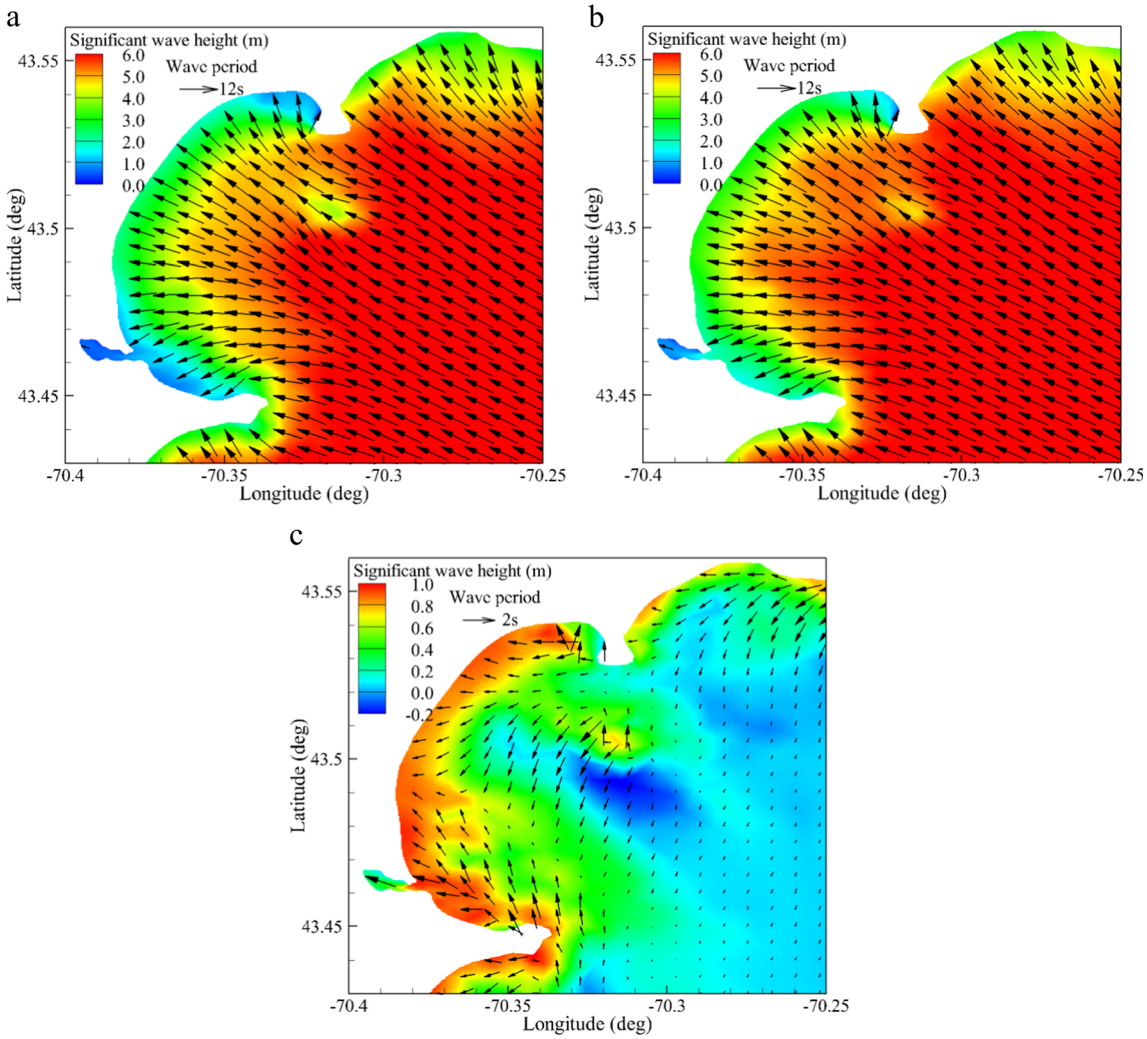

Fig. 16 Wave field in Saco Bay at 1400UTC April 16, 2007. **a** Without tide-surge effect. **b** With tide-surge effect. **c** The difference of wave height and wave direction with and without tide-surge effect, in which the *red color* indicates the increase of wave height by tide-surge effect while the *blue color* indicates the decrease of wave height

wave height change drastically, its impact on mean current and water level in the deep ocean is negligible. In the deep water, the 2-D model may not be adequate and the 3-D modeling approach incuding depth-dependent radiation stress such as those proposed by Mellor (2005) and Smith (2006) is required to resolve the wave-current interaction properly.

Acknowledgments This work was supported by the Maine Sea Grant and National Oceanic and Atmospheric Administration (Grants No. NA10OAR4170072). The work was also part of the Ensemble Estimation of Flood Risk in A Changing Climate (EFRaCC) project funded by the British Council under its Global Innovation Initiative, and the open fund research at the State Key Laboratory of Hydraulics and Mountain River (SKHL) at Sichuan University. We would like to thank John Cannon and Anthony Mignone at National Weather Service for helpful discussions. The second author is also supported on a summer assistantship by National Science Foundation award #IIA-1355457 to Maine EPSCoR at the University of Maine.

References

Ardhuin F, Rascle N, Belibassakis KA (2008) Explicit wave-averaged primitive equations using a generalized Lagrangian mean. Ocean Model 20(1):35–60. doi:10.1016/j.ocemod.2007.07.001

Beardsley R, Chen C, Xu Q (2013) Coastal flooding in Scituate (MA): a FVCOM study of the Dec. 27, 2010 nor'easter. J Geophys Res-Oceans 118:6030–6045. doi:10.1002/2013JC008862

Bennis AC, Ardhuin F, Dumas F (2011) On the coupling of wave and three-dimensional circulation models: choice of theoretical framework, practical implementation and adiabatic tests. Ocean Model 40(3):260–272. doi:10.1016/j.ocemod.2011.09.003

Bernier NB, Thompson KR (2007) Tide-surge interaction off the east coast of Canada and northeastern United States. J Geophys Res-Oceans 112:C06008. doi:10.1029/2006JC003793

Blain CA, Westerink JJ, Luettich RA Jr (1994) The influence of domain size on the response characteristics of a hurricane storm surge model. J Geophys Res-Oceans 99(C9):18467–18479. doi:10.1029/94JC01348

Bolaños R, Brown JM, Souza AJ (2014) Wave–current interactions in a tide dominated estuary. Cont Shelf Res 87:109–123. doi:10.1016/j.csr.2014.05.009

Booij N, Ris RC, Holthuijsen LH (1999) A third-generation wave model for coastal regions: 1. Model description and validation. J Geophys Res-Oceans 104(C4):7649–7666. doi:10.1029/98JC02622

Brothers LL, Belknap DF, Kelley JT, Janzen CD (2008) Sediment transport and dispersion in a cool-temperate estuary and embayment, Saco River estuary, Maine, USA. Mar Geol 251(3):183–194. doi:10.1016/j.margeo.2008.02.004

Brown JM, Wolf J (2009) Coupled wave and surge modelling for the eastern Irish Sea and implications for model wind-stress. Cont Shelf Res 29(10):1329–1342. doi:10.1016/j.csr.2009.03.004

Brown JM, Bolaños R, Wolf J (2013) The depth-varying response of coastal circulation and water levels to 2D radiation stress when applied in a coupled wave–tide–surge modelling system during an extreme storm. Coast Eng 82:102–113. doi:10.1016/j.coastaleng.2013.08.009

Bunya S, Dietrich JC, Westerink JJ, Ebersole BA, Smith JM, Atkinson JH, Jensen R, Resio DT, Luettich RA Jr, Dawson C, Cardone VJ, Cox AT, Powell MD, Westerink HJ, Roberts HJ (2010) A high-resolution coupled riverine flow, tide, wind, wind wave, and storm surge model for southern Louisiana and Mississippi. Part I: model development and validation. Mon Weather Rev 138(2):345–377. doi:10.1175/2009MWR2906.1

Charnock H (1955) Wind stress on a water surface. Q J Roy Meteor Soc 81(350):639–640. doi:10.1002/qj.49708135027

Chen C, Beardsley RC, Luettich RA Jr, Westerink JJ, Wang H, Perrie W, Toulany B (2013) Extratropical storm inundation testbed: intermodel comparisons in Scituate, Massachusetts. J Geophys Res-Oceans 118:5054–5073. doi:10.1002/jgrc.20397

Chen Q, Wang L, Tawes R (2008) Hydrodynamic response of northeastern Gulf of Mexico to hurricanes. Estuar Coast 31(6):1098–1116. doi:10.1007/s12237-008-9089-9

Christoffersen JB, Jonsson IG (1985) Bed friction and dissipation in a combined current and wave motion. Ocean Eng 12(5):387–423. doi:10.1016/0029-8018(85)90002-2

Craig PD, Banner ML (1994) Modeling wave-enhanced turbulence in the ocean surface layer. J Phys Oceanogr 24(12):2546–2559. doi:10.1175/1520-0485(1994)024<2546:MWETIT>2.0.CO;2

Dietrich JC, Bunya S, Westerink JJ, Ebersole BA, Smith JM, Atkinson JH, Jensen R, Resio DT, Luettich RA Jr, Dawson C, Cardone VJ, Cox AT, Powell MD, Westerink HJ, Roberts HJ (2010) A high-resolution coupled riverine flow, tide, wind, wind wave, and storm surge model for southern Louisiana and Mississippi. Part II: synoptic description and analysis of hurricanes Katrina and Rita. Mon Weather Rev 138(2):378–404. doi:10.1175/2009MWR2907.1

Dietrich JC, Tanaka S, Westerink JJ, Dawson CN, Luettich RA Jr, Zijlema M, Smith JM, Westerink LG, Westerink HJ (2012) Performance of the unstructured-mesh, SWAN + ADCIRC model in computing hurricane waves and surge. J Sci Comput 52(2):468–497. doi:10.1007/s10915-011-9555-6

Dietrich JC, Zijlema M, Westerink JJ, Holthuijsen LH, Dawson C, Luettich RA Jr, Stone GW (2011) Modeling hurricane waves and storm surge using integrally-coupled, scalable computations. Coast Eng 58(1):45–65. doi:10.1016/j.coastaleng.2010.08.001

Fry B (1988) Food web structure on Georges Bank from stable C, N, and S isotopic compositions. Limnol Oceanogr 33(5):1182–1190. doi:10.4319/lo.1988.33.5.1182

Garratt JR (1977) Review of drag coefficients over oceans and continents. Mon Weather Rev 105(7):915–929. doi:10.1175/1520-0493(1977)105<0915:RODCOO>2.0.CO;2

Grant WD, Madsen OS (1979) Combined wave and current interaction with a rough bottom. J Geophys Res-Oceans 84(C4):1797–1808. doi:10.1029/JC084iC04p01797

Greenberg DA (1983) Modelling the mean barotropic circulation in the Bay of Fundy and Gulf of Maine. J Phys Oceanogr 13(5):886–904. doi:10.1175/1520-0485(1983)013<0886:MTMBCI>2.0.CO;2

Hasselmann K, Barnett TP, Bouws E, Carlson H, Cartwright DE, Enke K, Ewing JA, Gienapp H, Hasselmann DE, Kruseman P et al (1973) Measurements of wind-wave growth and swell decay during the Joint North Sea Wave Project (JONSWAP). Deutches Hydrographisches Institute, Delft

Haus BK (2007) Surface current effects on the fetch-limited growth of wave energy. J Geophys Res-Oceans 112:C03003. doi:10.1029/2006JC003924

Hill HW, Kelley JT, Belknap DF, Dickson SM (2004) The effects of storms and storm-generated currents on sand beaches in southern Maine, USA. Mar Geol 210(1):149–168. doi:10.1016/j.margeo.2004.05.008

Janssen PA (1989) Wave-induced stress and the drag of air flow over sea waves. J Phys Oceanogr 19(6):745–754. doi:10.1175/1520-0485(1989)019<0745:WISATD>2.0.CO;2

Janssen PA (1991) Quasi-linear theory of wind-wave generation applied to wave forecasting. J Phys Oceanogr 21(11):1631–1642. doi:10.1175/1520-0485(1991)021<1631:QLTOWW>2.0.CO;2

Jenkins AD (1986) A theory for steady and variable wind-and wave-induced currents. J Phys Oceanogr 16(8):1370–1377. doi:10.1175/1520-0485(1986)016<1370:ATFSAV>2.0.CO;2

Jenkins AD (1987a) A Lagrangian model for wind-and wave-induced near-surface currents. Coast Eng 11(5):513–526. doi:10.1175/1520-0485(1986)016<1370:ATFSAV>2.0.CO;2

Jenkins AD (1987b) Wind and wave induced currents in a rotating sea with depth-varying eddy viscosity. J Phys Oceanogr 17(7):938–951. doi:10.1175/1520-0485(1987)017<0938:WAWICI>2.0.CO;2

Jenkins AD (1989) The use of a wave prediction model for driving a near-surface current model. Deutsche Hydrografische Zeitschrift 42(3–6):133–149. doi:10.1007/BF02226291

Johnson HK, Højstrup J, Vested HJ, Larsen SE (1998) On the dependence of sea surface roughness on wind waves. J Phys Oceanogr 28(9):1702–1716. doi:10.1175/1520-0485(1998)028<1702:OTDOSS>2.0.CO;2

Kelley JT, Barber DC, Belknap DF, FitzGerald DM, van Heteren S, Dickson SM (2005) Sand budgets at geological, historical and contemporary time scales for a developed beach system, Saco Bay, Maine, USA. Mar Geol 214(1):117–142. doi:10.1016/j.margeo.2004.10.027

Komen GJ, Cavaleri L, Donelan M, Hasselmann K, Hasselmann S, Janssen PAEM (1996) Dynamics and modelling of ocean waves. Cambridge university press, Cambridge

Longuet-Higgins MS, Stewart RW (1961) The changes in amplitude of short gravity waves on steady non-uniform currents. J Fluid Mech 10:529–549. doi:10.1017/S0022112061000342

Longuet-Higgins MS, Stewart RW (1962) Radiation stress and mass transport in gravity waves, with application to “surf beats”. J Fluid Mech 13:481–504. doi:10.1017/S0022112062000877

Longuet-Higgins MS, Stewart RW (1964) Radiation stresses in water waves; a physical discussion, with applications. Deep-Sea Res 11(4):529–562. doi:10.1016/0011-7471(64)90001-4

Luettich RA Jr, Westerink JJ (2006) ADCIRC: A (parallel) advanced circulation model for oceanic, coastal and estuareine waters; users manual for version 51. http://adcirc.org/home/documentation/users-manual-v51

Luettich RA Jr, Hu S, Westerink JJ (1994) Development of the direct stress solution technique for three-dimensional hydrodynamic models using finite elements. Int J Numer Methods Fluids 19(4):295–319. doi:10.1002/fld.1650190403

Luettich RA Jr, Westerink JJ, Scheffner NW (1992) ADCIRC: an advanced three-dimensional circulation model for shelves, coasts and estuaries. Report 1. Theory and methodology of ADCIRC-2DDI and ADCIRC-3DL. U.S. Army Corps of Engineers Technical Report DRP-92-6. http://oai.dtic.mil/oai/oai?verb=getRecord&metadataPrefix=html&identifier=ADA261608

Marrone JF (2008) Evaluation of impacts of the Patriots' Day storm (April 15–18, 2007) on the New England coastline. Solutions to Coastal Disasters: 507–517. doi: 10.1061/40968(312)46

Mellor G (2005) Some consequences of the three-dimensional current and surface wave equations. J Phys Oceanogr 35(11):2291–2298. doi:10.1175/JPO2794.1

Mellor G (2008) The depth-dependent current and wave interaction equations: a revision. J Phys Oceanogr 38(11):2587–2596. doi:10.1175/2008JPO3971.1

Moon IJ, Ginis I, Hara T (2004b) Effect of surface waves on air-sea momentum exchange. Part II: behavior of drag coefficient under tropical cyclones. J Atmos Sci 61(19):2334–2348. doi:10.1175/1520-0469(2004)061<2334:EOSWOA>2.0.CO;2

Moon IJ, Hara T, Ginis I, Belcher SE, Tolman HL (2004a) Effect of surface waves on air-sea momentum exchange. Part I: effect of mature and growing seas. J Atmos Sci 61(19):2321–2333. doi:10.1175/1520-0469(2004)061<2321:EOSWOA>2.0.CO;2

Mukai AY, Westerink JJ, Luettich RA Jr, Mark D (2001) Eastcoast2001, a tidal constituent database for the Western North Atlantic Ocean, Gulf of Mexico and Caribbean Sea. Technical Report ERDC/CHL TR-02-24, U.S. Army Corps of Engineers. http://oai.dtic.mil/oai/oai?verb=getRecord&metadataPrefix=html&identifier=ADA408733

Nicolle A, Karpytchev M, Benoit M (2009) Amplification of the storm surges in shallow waters of the Pertuis Charentais (Bay of Biscay, France). Ocean Dyn 59(6):921–935. doi:10.1007/s10236-009-0219-0

Ozer P, Padilla-Hernández R, Monbaliu J, Fanjul EA, Albiach JCC, Osuna P, Yu JCS, Wolf J (2000) A coupling module for tides, surges and waves. Coast Eng 41(1–3):95–124. doi:10.1016/S0378-3839(00)00028-4

Panchang VG, Jeong C, Li D (2008) Wave climatology in coastal Maine for aquaculture and other applications. Estuar Coast 31(2):289–299. doi:10.1007/s12237-007-9016-5

Pawlowicz R, Beardsley B, Lentz S (2002) Classical tidal harmonic analysis including error estimates in MATLAB using T_TIDE. Comput Geosci 28(8):929–937. doi:10.1016/S0098-3004(02)00013-4

Perrie W, Tang CL, Hu Y, DeTracy BM (2003) The impact of waves on surface currents. J Phys Oceanogr 33(10):2126–2140. doi:10.1175/1520-0485(2003)033<2126:TIOWOS>2.0.CO;2

Pettigrew NR, Churchill JH, Janzen CD, Mangum LJ, Signell RP, Thomas AC, Townsend DW, Wallinga JP, Xue H (2005) The kinematic and hydrographic structure of the Gulf of Maine coastal current. Deep-Sea Res Pt II 52(19):2369–2391. doi:10.1016/j.dsr2.2005.06.033

Ris RC, Holthuijsen LH, Booij N (1999) A third-generation wave model for coastal regions: 2. Verification. J Geophys Res-Oceans 104(C4):7649–7666. doi:10.1029/1998JC900123

Sheng YP, Liu T (2011) Three-dimensional simulation of wave-induced circulation: comparison of three radiation stress formulations. J Geophys Res-Oceans 116:C05021. doi:10.1029/2010JC006765

Smith JA (2006) Wave-current interactions in finite depth. J Phys Oceanogr 36(7):1403–1419. doi:10.1175/JPO2911.1

Sun Y, Chen C, Beardsley RC, Xu Q, Qi J, Lin H (2013) Impact of current-wave interaction on storm surge simulation: a case study for hurricane Bob. J Geophys Res-Oceans 118(5):2685–2701. doi:10.1002/jgrc.20207

Sverdrup HU, Johnson MW, Fleming RH (1942) The oceans: their physics, chemistry, and general biology. Prentice-Hall, New York

Tang CL, Perrie W, Jenkins AD, DeTracey BM, Hu Y, Toulany B, Smith PC (2007) Observation and modeling of surface currents on the Grand Banks: a study of the wave effects on surface currents. J Geophys Res-Oceans 112:C10025. doi:10.1002/jgrc.20207

Taylor PK, Yelland MJ (2001). The dependence of sea surface roughness on the height and steepness of the waves. J Phys Oceanogr 31(2):572–590. dio: 10.1175/1520-0485(2001)031<0572:TDOSSR>2.0.CO;2

Tilburg CE, Gill SM, Zeeman SI, Carlson AE, Arienti TW, Eickhorst JA, Yund PO (2011) Characteristics of a shallow river plume: observations from the Saco River coastal observing system. Estuar Coast 34(4):785–799. doi:10.1007/s12237-011-9401-y

Uchiyama Y, McWilliams JC, Restrepo JM (2009) Wave-current interaction in nearshore shear instability analyzed with a vortex force formalism. J Geophys Res-Oceans 114:C06021. doi:10.1029/2008JC005135

Uchiyama Y, McWilliams JC, Shchepetkin AF (2010) Wave–current interaction in an oceanic circulation model with a vortex-force formalism: application to the surf zone. Ocean Model 34(1):16–35. doi:10.1016/j.ocemod.2010.04.002

Warner JC, Armstrong B, He R, Zambon JB (2010) Development of a coupled ocean–atmosphere–wave–sediment transport (COAWST) modeling system. Ocean Model 35(3):230–244. doi:10.1016/j.ocemod.2010.07.010

Warner JC, Butman B, Dalyander PS (2008) Storm-driven sediment transport in Massachusetts Bay. Cont Shelf Res 28(2):257–282. doi:10.1016/j.csr.2007.08.008

Westerink JJ, Luettich RA Jr, Blain CA, Scheffner NW (1994) ADCIRC: an advanced three-dimensional circulation model for shelves, coasts and estuaries. Report 2: users' manual for ADCIRC-2DDI. Technical Report DRP-92-6, U.S. Army Corps of Engineers. http://www.unc.edu/ims/adcirc/publications/1994/1994_Westerink01.pdf

Westerink JJ, Luettich RA Jr, Feyen JC, Atkinson JH, Dawson C, Roberts HJ, Powell MD, Dunion JP, Kubatko EJ, Pourtaheri H (2008) A basin-to channel-scale unstructured grid hurricane storm surge model applied to southern Louisiana. Mon Weather Rev 136(3):833–864. doi:10.1175/2007MWR1946.1

Wolf J (2009) Coastal flooding: impacts of coupled wave–surge–tide models. Nat Hazards 49(2):241–260. doi:10.1007/s11069-008-9316-5

Xia H, Xia Z, Zhu L (2004) Vertical variation in radiation stress and wave-induced current. Coast Eng 51(4):309–321. doi:10.1016/j.coastaleng.2004.03.003

Xie L, Wu K, Pietrafesa L, Zhang C (2001) A numerical study of wave-current interaction through surface and bottom stresses: wind-driven circulation in the South Atlantic Bight under uniform winds. J Geophys Res-Oceans 106(C8):16841–16855. doi:10.1029/2000JC000292

Xie D, Zou Q, Cannon JW (2016) Application of SWAN + ADCIRC to tide-surge and wave simulation in Gulf of Maine during Patriot's Day storm. WSE 9(1):33–41. doi:10.1016/j.wse.2016.02.003

Xue HJ, Chai F, Pettigrew NR (2000) A model study of the seasonal circulation in the Gulf of Maine. J Phys Oceanogr 30(5):1111–1135. doi:10.1175/1520-0485(2000)030<1111:AMSOTS>2.0.CO;2

Yang Z, Myers E (2008) Barotropic tidal energetics and tidal datums in the Gulf of Maine and Georges Bank region. Estuar Coast Model (2007):74–94. doi:10.1061/40990(324)5

Zijlema M (2010) Computation of wind-wave spectra in coastal waters with SWAN on unstructured grids. Coast Eng 57(3):267–277. doi:10.1016/j.coastaleng.2009.10.011

Zijlema M, van Vledder GP, Holthuij Sen LH (2012) Bottom friction and wind drag for wave models. Coast Eng 65:19–26. doi:10.1016/j.coastaleng.2012.03.002

Zou Q (2004) A simple model for random wave bottom friction and dissipation. J Phys Oceanogr 34(6):1459–1467. doi:10.1175/1520-0485(2004)034<1459:ASMFRW>2.0.CO;2

Zou Q, Bowen AJ, Hay AE (2006) The vertical distribution of wave shear stress in variable water depth: theory and field observations. J Geophys Res-Oceans 111:C09032. doi:10.1029/2005JC003300

Zou Q, Chen Y, Cluckie I, Hewston R, Pan S, Peng Z, Reeve D (2013) Ensemble prediction of coastal flood risk arising from overtopping by linking meteorological, ocean, coastal and surf zone models. Q J Roy Meteor Soc 139(671):298–313. doi:10.1002/qj.2078